Characterization of temperature criteria using gas-phase fuel streams for MILD coal combustion

Hang Zhou*, Josh McConnell, Terry A. Ring, James C. Sutherland*

Department of Chemical Engineering, University of Utah, Salt Lake City, UT, United States

Abstract

MILD combustion is achieved when the reactants' inlet temperature (T_{inlet}) is higher than the self-ignition temperature of the reactants ($T_{\text{self-ignition}}$) and the temperature increase upon reaction ($\Delta T = T_{\max} - T_{\text{inlet}}$) is lower than $T_{\text{self-ignition}}$. The method to get T_{inlet} and $T_{\text{self-ignition}}$ is ambiguous for coal combustion because the multiple fuel streams are released from coal particles through vaporization, devolatilization, tar/soot reaction and char oxidation/gasification at different temperatures and different times as the particles heat up. We propose a method to determine the gas-phase fuel streams in coal combustion using the reaction rate of each subprocess and gas and particle temperature profiles in the reactor before ignition. The mixture of fuel streams and oxidizer is used to get T_{inlet} and $T_{\text{self-ignition}}$ for the temperature criteria for MILD coal combustion. By way of example, this method is applied to identify the required dilution rate needed to reach MILD coal combustion conditions for two types of coal. It is observed that MILD coal combustion is achieved when the dilution rate, K_v, is larger than 0.5 for $T_{\text{oxid}} = 1200$K and 1.0 for $T_{\text{oxid}} = 350$K. Three tar/soot treatments give similar predictions of the required recirculation rate to reach MILD coal combustion conditions, even for a simplified model that uses C_2H_2 for tar while neglecting the formation of soot.

Keywords:

MILD Coal Combustion, Temperature Criteria, Fuel Stream, Tar/Soot Treatment

1. Introduction

Moderate or Intense Low-oxygen Dilution combustion (MILD), characterized by a non-visible flame, lower peak temperature and lower NO_x emissions, has attracted increasing attention in both experimental and numerical investigations [1–4]. Cavaliere, et al. [1] proposed the definition of MILD combustion based on the analysis of methane combustion in perfectly-stirred reactors: "A combustion process is named MILD when the inlet temperature of the reactant mixture is higher than mixture self-ignition temperature whereas the maximum allowable temperature increase

*Corresponding author:

Email addresses: hang.zhou@chemeng.utah.edu (Hang Zhou), James.Sutherland@chemeng.utah.edu (James C. Sutherland)

with respect to inlet temperature during combustion is lower than mixture self-ignition temperature(in Kelvin),"

$$T_{\mathrm{inlet}} > T_{\mathrm{self-ignition}}, \tag{1}$$

$$(T_{\mathrm{max}} - T_{\mathrm{inlet}}) < T_{\mathrm{self-ignition}}. \tag{2}$$

This criteria is the most common definition of MILD combustion and will be used for this investigation of MILD coal combustion.

Although the application of the aforementioned temperature criteria is straightforward for gas-phase combustion, it is ambiguous for coal combustion because the fuel stream composition and temperature are not well-defined. In experiments of MILD coal combustion [5–9], the criterion (1) is satisfied by preheating the reactor, usually by the combustion of natural gas, to have the initial temperature higher than the approximate coal particle self-ignition temperature. However, the inlet temperature of the mixture of fuel and oxidizer is not actually measured and compared with the self-ignition temperature. The method and composition of the reactants used to get self-ignition temperature, which is set approximately (based on the coal type or experience, and is usually around 1100K), are not defined clearly.

Considering gas-phase combustion only, the 'inlet' temperature corresponds to the mixture of oxidizer and fuel, which originates from the coal particle whose temperature evolves over time. The gas-phase fuel in coal combustion evolves from particles as a result of vaporization, devolatilization, tar/soot reaction and char oxidation/gasification occurring at *different* temperatures as the particle heats up over time. Defining a temperature and composition of the resulting gas-phase fuel stream that is suitable to characterize T_{inlet} and $T_{\mathrm{self-ignition}}$ is, therefore, not a trivial matter in the context of MILD coal combustion.

Due to the existence of multiple fuel streams arising from vaporization, devolatilization, tar/soot reaction and char gasification/oxidation, models considering gas-phase fuel generated from coal particle heat up are always applied with some assumptions. Vascellari, et al [10] represented the gas-phase fuel by one volatile stream from devolatilization to study the ignition of single particles in a laminar entrained-flow reactor. Watanabe, et al. [11] considered two fuel streams; one for volatile matter (CO, CH_4 and C_2H_2) and the other for char products, and extended it to three streams for moisture, volatile matter and char products in [12]. Rieth, et al. [13, 14] and Wen, et al. [15, 16] used a two fuel stream method for volatiles and char products with a more complex devolatilization model for a study of pulverized coal combustion in turbulent flows. McConnell, et al. [17] evaluated various tar/soot models by using two fuel streams for light gas from devolatilization and products from tar/soot reaction with a steady laminar flamelet model. All the aforementioned research provides guidance for getting gas-phase fuel streams from coal combustion, which can be applied to the temperature criteria of MILD coal combustion.

The main objective of this paper is to propose a method to determine the gas-phase fuel stream temperature and composition in coal combustion, which determines the inlet and self-ignition temperature used in the criteria for MILD combustion. We use detailed kinetic treatments for devolatilization, char gasification/oxidation and gas-phase chemistry with fully coupled mass and energy exchange between particles and the gas phase to provide detailed information about the evolution of composition and temperature of the fuel stream originating from the coal particle. We also address the impacts of tar/soot treatment, coal type and oxidizer temperature on the temperatures and compositions of fuel streams. This is the first work providing these clarifications on the application of MILD temperature criteria to coal combustion.

2. Modeling Description

Because of the transient processes of particle heating, vaporization, devolatilization and char reaction of coal particles along the reactor, spatial gradients of temperature/species fields along the reactor are observed in MILD coal combustion [8, 9, 18]. To model the spatial distribution, we consider an open (constant pressure) multi-phase plug flow reactor (PFR) at steady state, as depicted in Figure 1. The remainder of this section describes the governing equations for this system and then describes the simulations performed herein.

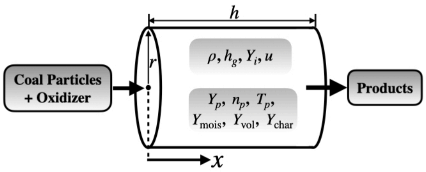

Figure 1: Configuration of multi-phase Plug Flow Reactor

2.1. *Governing equations for multi-phase PFR*

2.1.1. *Gas-phase governing equations*

The governing equations are derived in Appendix A, and are summarized here. The conservation equations for gas-phase density (ρ_g), axial velocity (u), species mass fractions (Y_i) and specific enthalpy (h_g) are given as

$$\frac{d\rho_g}{dx} = \frac{1}{u^2}\frac{dp}{dx} + \frac{2S_{m_g}}{u} \tag{3}$$

$$\frac{du}{dx} = -\frac{1}{\rho_g u}\frac{dp}{dx} - \frac{S_{m_g}}{\rho_g} \tag{4}$$

$$\frac{dY_i}{dx} = \frac{\omega_i + S_{Y_i} - Y_i S_{m_g}}{\rho_g u} \tag{5}$$

$$\frac{dh_g}{dx} = \frac{Q_g + S_{h_g} - h_g S_{m_g}}{\rho_g u} + \frac{1}{\rho_g}\frac{dp}{dx} \tag{6}$$

where ω_i is the species volumetric reaction rate. S_{h_g}, S_{m_g} and S_{Y_i} are the interphase exchange terms for specific enthalpy, total mass of gas phase and mass fraction of i^{th} species respectively (see §2.2-§2.3). $Q_g = {}^{kA}/_{V}(T_{\inf} - T_g) + Q_{pg}$

includes the heat transfer between gas phase, T_g, and surroundings, T_{inf}, and between gas phase and particles, Q_{pg} (see (14)). Here, k, A and V denote the convective coefficient, reactor surface area and volume. $\frac{dp}{dx}$ is calculated using ideal gas law, $p = \rho_g R T_g / M_w$, as shown in (A.13)-(A.16) in Appendix A.

2.1.2. Particle-phase governing equations

We model particles as a continuous (though separate) phase. For each particle size, j, equations (7)-(8) are solved for number of particles per *gas* mass, $n_{p,j}$, particle temperature $T_{p,j}$ and total mass of particles per *gas* mass $Y_{p,j}$:

$$\frac{dn_{p,j}}{dx} = -\frac{n_{p,j} S_{m_g}}{\rho_g u} \tag{7}$$

$$\frac{dY_{p,j}}{dx} = \frac{S_{m_{p,j}} - Y_{p,j} S_{m_g}}{\rho_g u} \tag{8}$$

$$\frac{dT_{p,j}}{dx} = \frac{Q_{p,j} + S_{h_{p,j}}}{\rho_g u Y_{p,j} C_{p,p,j}} \tag{9}$$

where $C_{p,p,j}$ is the heat capacity of particles with j^{th} particle size, calculated as

$$C_{p,p,j} = \sum_{\beta} \frac{Y_{\beta,j}}{Y_{p,j}} C_{p\beta,j} \tag{10}$$

where $\beta = \{\mathrm{mois}, \mathrm{vol}, \mathrm{char}, \mathrm{ash}\}$ for moisture, volatiles, char and ash respectively and $Y_{\beta,j}$ is the mass of constituent β per mass of *gas*. The heat capacity of each coal constituent, $C_{p\beta,j}$, is obtained based on [19, 20]. The governing equations for moisture mass ($Y_{\mathrm{mois},j}$) and char mass ($Y_{\mathrm{char},j}$) in particles per *gas* mass with j^{th} particle size have the same format as (8). The volatile mass per *gas* mass, $Y_{\mathrm{vol},j}$, is calculated within devolatilization model (see §2.2.2). The ash mass per *gas* mass is obtained by difference:

$$Y_{\mathrm{ash},j} = Y_{p,j} - Y_{\mathrm{mois},j} - Y_{\mathrm{vol},j} - Y_{\mathrm{char},j} \tag{11}$$

Particle heat transfer is described by the following expression,

$$Q_{p,j} = -Q_{pg,j} + \varepsilon_{pw}\sigma A_{p,j}/V (T_{\mathrm{inf}}^4 - T_{p,j}^4), \tag{12}$$

and includes the heat transfer between the gas and particle phases as well as radiative heat transfer between the particles and the surroundings at temperature T_{inf}. Heat transfer between gas and particles, which includes convective and radiative terms, is described by

$$Q_{pg,j} = \frac{h_{pg,j} A_{p,j}}{V}(T_{p,j} - T_g) + \frac{\varepsilon_{pg}\sigma A_{p,j}}{V}(T_{p,j}^4 - T_g^4) \tag{13}$$

$$Q_{pg} = \sum_{j=1}^{n_{\mathrm{size}}} Q_{pg,j} \tag{14}$$

where $h_{pg,j} = {}^{k_g \mathrm{Nu}}/_{d_{p,j}}$ is the convective heat transfer coefficient between gas and particles, with $\mathrm{Nu} = 2{+}0.6\mathrm{Re}_p^{1/2}\mathrm{Pr}^{1/3}$ [21] and k_g representing the thermal conductivity of gas. $\varepsilon_{pg} = 0.2$ and $\varepsilon_{pw} = 0.8$ are the emissivities, and σ is Stefan–Boltzmann constant. $A_{p,j} = \pi d_{p,j}^2 N_{p,j}$ is the total surface area of particles with j^{th} size, with $N_{p,j} = \rho_g V n_{p,j}$ representing the total number of j^{th} particles. $d_{p,j}$ is the j^{th} particle diameter, which is assumed to be constant during reaction. n_{size} donates the number of particle sizes used in the calculation. $S_{m_{p,j}}$ and $S_{h_{p,j}}$ are the interphase exchange terms for total particle mass and the total reaction heat from vaporization, devolatilization and char oxidation/gasification of particles with j^{th} size respectively (see §2.2).

2.2. Coal particle sub-models

Pulverized coal combustion is modeled using four well-defined steps, namely, vaporization, devolatilization, tar and soot combustion, and char oxidation/gasification. No temporal ordering of these four steps is imposed in our model. Models describing each step are introduced in this section.

2.2.1. Vaporization model

The vaporization rate of moisture content in coal particles with j^{th} size is given as

$$S_{m_{\mathrm{mois}},j} = k_v \left(\frac{P_{\mathrm{H_2O,sat},j}}{RT_{p,j}} - \frac{P_{\mathrm{H_2O}}}{RT_g} \right) A_{p,j} M_{w,\mathrm{H_2O}} \tag{15}$$

where k_v is the mass transfer coefficient of steam into air [22]. $P_{\mathrm{H_2O,sat},j}$ is the saturation pressure of H_2O at particle temperature. $P_{\mathrm{H_2O}}$ is the partial pressure of H_2O in the gas phase. R and $M_{w,\mathrm{H_2O}}$ are the ideal gas constant and molecular weight of H_2O. The species source term of H_2O and particle temperature source term contributed from vaporization is

$$S_{Y_{\mathrm{H_2O}}}^{\mathrm{vap}} = -\sum_{j=1}^{n_{\mathrm{size}}} S_{m_{\mathrm{mois}},j} \tag{16}$$

$$S_{h_{p,j}}^{\mathrm{vap}} = S_{m_{\mathrm{mois}},j} \lambda_{\mathrm{vap}} \tag{17}$$

λ_{vap} represents the water's latent heat of vaporization.

2.2.2. Devolatilization model

Chemical Percolation and Devolatilization (CPD) model is utilized for devolatilization. It models the coal structure transformation as the decomposition of labile bridges (l) to highly reactive intermediate bridges (l^*), which further react to produce either light gases (CH_4, CO, CO_2, H_2, H_2O, NH_3, and HCN), char and tar, or side chains (δ_k) that eventually convert into light gases and tar. Light gases and tar are included in g_k in (18).

$$l \rightarrow l^* \begin{array}{l} \nearrow \delta_k \rightarrow g_k \\ \searrow \mathrm{char} + g_k \end{array} \tag{18}$$

The governing equations for the mass of l, δ_k and g_k per *gas* mass ($Y_{l,j}$, $Y_{\delta_k,j}$ and $Y_{g_k,j}$) for particles with j^{th} size have the same format as (8). Details about calculating source terms of $S_{m_{l,j}}$, $S_{m_{\delta_k,j}}$, $S_{m_{g_k,j}}$ and $S^{\text{vol}}_{m_{\text{char}},j}$ can be found in [23, 24].

The volatile mass per *gas* mass, $Y_{\text{vol},j}$, and its reaction rate are

$$Y_{\text{vol},j} = Y_{l,j} + \sum_k Y_{\delta_k,j} \tag{19}$$

$$S_{m_{\text{vol}},j} = S^{\text{vol}}_{m_{\text{char}},j} + \sum_k S_{m_{g_k},j} \tag{20}$$

The species source terms contributed from devolatilization, $S^{\text{dev}}_{Y_i}$, is calculated by adding $S_{m_{g_k,j}}$ for i^{th} species from all particle sizes. The reaction heat of devolatilization is not considered in this work, $S^{\text{dev}}_{h_p,j} = 0$.

2.2.3. Tar and soot model

Tar is composed of various high molecular weight hydrocarbon species, while soot is composed of small carbonaceous particles [25]. In scenarios involving coal combustion, tar is the primary precursor to soot. Empirical treatment of tar and soot is utilized to avoid using large, computationally-intensive, chemical mechanisms [26]. Considering different tar/soot treatments yield different gas-phase species from the tar/soot reactions and predict different temperatures in the reactor [17], three empirical models are used in this work for tar and soot treatment. Details of each of the models can be found in an assessment of three models by McConnell, et al. [17].

Model 1: C_2H_2. The first model is a simplified model assuming tar as acetylene (C_2H_2) and neglecting the formation of soot. This model has been proven to give good agreement with experimental results for the ignition delay [27] and flame standoff [28]. By making this assumption, no additional model for tar/soot reaction is required since C_2H_2 is included in the chemical mechanism (GRI 2.11).

Model 2: $C_{10}H_{10}$+C. The second model is based on the model developed by [29, 30]. This approach assumes that tar is dihydronaphthalene ($C_{10}H_{10}$) and soot is carbon. CO and H_2O are assumed to be the products of tar/soot oxidation, which gives the following reaction scheme:

$$\text{tar}(C_{10}H_{10}) \rightarrow 10\text{soot}(C) + 5H_2. \tag{21a}$$

$$\text{tar}(C_{10}H_{10}) + {}^{15}/_{2}O_2 \rightarrow 10\,CO + 5\,H_2O, \tag{21b}$$

$$\text{soot}(C) + {}^{1}/_{2}O_2 \rightarrow CO. \tag{21c}$$

Model 3: $C_{10}H_{10}$. The third model applies the same assumption for tar as *Model 2*, and assumes soot has the same empirical formula ($C_{10}H_{10}$) as tar. This results in the following reaction scheme

$$\text{tar}(C_{10}H_{10}) \rightarrow \text{soot}(C_{10}H_{10}). \tag{22a}$$

$$\text{tar}(C_{10}H_{10}) + {}^{15}\!/\!_{2}O_2 \rightarrow 10\,CO + 5\,H_2O, \tag{22b}$$

$$\text{soot}(C_{10}H_{10}) + {}^{15}\!/\!_{2}O_2 \rightarrow 10\,CO + 5\,H_2O. \tag{22c}$$

As stated in [17], the motivation for assuming soot has the same empirical formula as tar is that it facilitates incorporation with mixture fraction based models, and we consider *Model 3* here because of its potential for application to MILD coal combustion systems. *Model 3* predicts a maximum temperature ∼100K higher than that from *Model 2* observed in [17], which affects the achievement of MILD combustion as shown in (2). Additionally, CO and H_2O without H_2 are released from *Model 3*, compared with *Model 2*. This predicts different compositions of gas-phase fuel from tar/soot reactions, and may give different inlet and self-ignition temperatures in (1) and (2) (see §3). Therefore, the prediction of MILD combustion is compared between *Model 2* and *Model 3*.

For models 2 and 3, equations for mass of tar and soot per *gas* mass, having the same format as (8), are solved. More details of the reaction kinetics, including the rate of soot formation $S^{\text{tarToSoot}}_{m_{\text{tar}}}$, tar oxidation $S^{\text{oxid}}_{m_{\text{tar}}}$ and soot oxidation $S^{\text{oxid}}_{m_{\text{soot}}}$, in (21) and (22), and species source term, $S^{\text{tar,soot}}_{Y_i}$ can be found in [30] and [17].

2.2.4. *Char oxidation/gasification model*

Char oxidation and gasification are heterogeneous reactions at the particle surface. The rate of char oxidation for particles of j^{th} size is described as

$$S^{\text{oxid}}_{m_{\text{char}},j} = -\frac{r_{C,j} M_{w,C}}{\varphi_j} A_{p,j} \tag{23}$$

where $M_{w,C}$ is the molecular weight of carbon. $r_{C,j}$ is calculated by n^{th}-order Langmuir-Hinshelwood (n^{th}-order LH) model [31]:

$$r_{C,j} = \frac{k_{2,j} k_{1,j} P^n_{O_2,s,j}}{k_{1,j} P^n_{O_2,s,j} + k_{2,j}} \tag{24}$$

where $k_{1,j}$ and $k_{2,j}$ are Arrhenius rate constants depending on particle temperature. $P_{O_2,\text{s,j}}$ is the partial pressure of O_2 at particle surface, with $n = 0.3$.

φ_j denotes the stoichiometric ratio of carbon consumption [32], and is calculated by

$$\varphi_j = \frac{2(1 + (CO_2/CO)_j)}{1 + 2(CO_2/CO)_j} \tag{25}$$

where $(CO_2/CO)_j$ donates the moles ratio between CO_2 and CO produced by char oxidation. In this work, a model from Tognotti, *et al.*[33] is applied

$$\left(\frac{CO_2}{CO}\right)_j = A P^{n_r}_{O_2,s,j} \exp\left(\frac{B}{T_{p,j}}\right) \tag{26}$$

where $A = 0.02$, $B = 3070K$, $n_r = 0.21$ and $P_{\mathrm{O_2},s,j}$ is in atm. The rates of char oxidation producing CO and CO_2 are given, respectively, as:

$$S^{\mathrm{oxid,CO_2}}_{m_{\mathrm{char}},j} = \frac{(\mathrm{CO_2/CO})_j}{1 + (\mathrm{CO_2/CO})_j} S^{\mathrm{oxid}}_{m_{\mathrm{char}},j} \tag{27}$$

$$S^{\mathrm{oxid,CO}}_{m_{\mathrm{char}},j} = \frac{S^{\mathrm{oxid}}_{m_{\mathrm{char}},j}}{1 + (\mathrm{CO_2/CO})_j} \tag{28}$$

Char reacts with CO_2 and H_2O surrounding the particles during gasification:

$$\mathrm{C_{(s)} + CO_2 \rightarrow 2CO} \tag{29}$$

$$\mathrm{C_{(s)} + H_2O \rightarrow CO + H_2} \tag{30}$$

The 1st-order Arrhenius gasification model is implemented:

$$S^{\mathrm{gasif,H_2O}}_{m_{\mathrm{char}},j} = -A_{p,j} k_{\mathrm{H_2O},j} P_{\mathrm{H_2O},s,j} \tag{31}$$

$$S^{\mathrm{gasif,CO_2}}_{m_{\mathrm{char}},j} = -A_{p,j} k_{\mathrm{CO_2},j} P_{\mathrm{CO_2},s,j} \tag{32}$$

with $k_{\mathrm{H2O},j}$ and $k_{\mathrm{CO_2},j}$ representing the Arrhenius constants, and $P_{\mathrm{H_2O,s},j}$ and $P_{\mathrm{CO_2,s},j}$ representing the partial pressure of H_2O and CO_2 at particle surface. The Arrhenius parameters are taken from [34].

The source term of char mass in particles is given as

$$S_{m_{\mathrm{char},j}} = S^{\mathrm{vol}}_{m_{\mathrm{char}},j} + S^{\mathrm{oxid}}_{m_{\mathrm{char}},j} + S^{\mathrm{gasif,H_2O}}_{m_{\mathrm{char}},j} + S^{\mathrm{gasif,CO_2}}_{m_{\mathrm{char}},j} \tag{33}$$

The heat released from char oxidation/gasification is absorbed by both gas and particle phases. The energy-exchange term in particle temperature equation is given in terms of (27), (28), (31) and (32) as

$$\begin{aligned} S^{\mathrm{char}}_{h_p,j} = (1-\alpha) \sum_{i=\mathrm{CO,\,CO_2}} S^{\mathrm{oxid},i}_{m_{\mathrm{char}},j} \Delta H^{\mathrm{oxid}}_i \\ + (1-\alpha) \sum_{i=\mathrm{CO_2,\,H_2O}} S^{\mathrm{gasif},i}_{m_{\mathrm{char}},j} \Delta H^{\mathrm{gasif}}_i \end{aligned} \tag{34}$$

where ΔH_i is the enthalpy of the heterogeneous reactions [35]. $\alpha = 0.3$ is the percentage of energy released to gas phase, and $1 - \alpha$ is the percentage of energy absorbed by particles [28]. The corresponding energy-exchange term to gas phase is

$$S_{h_g}^{\mathrm{char}} = \alpha \sum_{i=\mathrm{CO},\,\mathrm{CO_2}} S_{m_{\mathrm{char}},j}^{\mathrm{oxid},i} \Delta H_i^{\mathrm{oxid}} + \alpha \sum_{i=\mathrm{CO_2},\,\mathrm{H_2O}} S_{m_{\mathrm{char}},j}^{\mathrm{gasif},i} \Delta H_i^{\mathrm{gasif}} \tag{35}$$

2.3. Source terms

The interphase exchange terms in (3)-(6) depend upon the choice of coal sub-models. The species source term in (5) and source term for the total mass of gas phase are given as

$$S_{Y_i} = S_{Y_i}^{\mathrm{vap}} + S_{Y_i}^{\mathrm{dev}} + S_{Y_i}^{\mathrm{tar,soot}} + +S_{Y_i}^{\mathrm{char}} \tag{36}$$

$$S_{m_g} = \sum_i S_{Y_i} \tag{37}$$

The source term for specific enthalpy of gas phase, S_{h_g}, includes the energy transported by gas species between particles and gas, reaction heat of tar and soot reactions if using tar/soot models 2 or 3, and reaction heat released from char oxidation/gasification $S_{h_g}^{\mathrm{char}}$:

$$S_{h_g} = \sum_i^{n_s} S_{Y_i} h_i + \sum_{p=\mathrm{tar,soot}} S_{m_p}^{\mathrm{oxid}} \Delta H_p + S_{h_g}^{\mathrm{char}} \tag{38}$$

where n_s is the number of species, h_i is the enthalpy of i^{th} species. ΔH_p is the reaction heat of tar/soot oxidation. It is assumed that all heat released from tar/soot oxidation is absorbed by gas phase.

The total exchange terms in particle mass and temperature equations are

$$S_{m_{p,j}} = S_{m_{\mathrm{mois}},j} + S_{m_{\mathrm{vol}},j} + S_{m_{\mathrm{char},j}} \tag{39}$$

$$S_{h_p,j} = S_{h_p,j}^{\mathrm{vap}} + S_{h_p,j}^{\mathrm{dev}} + +S_{h_p,j}^{\mathrm{char}} \tag{40}$$

2.4. Computational configuration

The governing equations described in §2.1 are solved using a fully-coupled scheme with an implicit, dual time-stepping method [36]. The PFR is a cylinder with a radius of 0.05 m and grid spacing of $\Delta x = 10^{-4}$ m, which provided grid-converged results, is applied. The GRI 2.11 mechanism [37] is utilized for gas-phase reactions. Two types of coals, Illinois #6 and Guizhou, with an initial temperature of 350K, particle size of 50 μm, and properties given in Table 1 are considered. The volatile contents in two coals are very different, which is important evaluating whether the method we proposed in this work can be applied to different coal types.

Air at T_{oxid} =1200K and 350K are used as the oxidizers, respectively, to study the effects of oxidizer temperature. An inlet velocity of 10 m/s for pure oxidizer is used, giving particle Reynolds number $\mathrm{Re}_p \approx 2$. The particle loading at the inlet is calculated using the mass flow rate of gas-phase and the overall equivalence ratio in the reactor, which is set to be unity.

To consider the effects of heat loss in the system, we add the convective heat transfer between the gas phase and the surroundings with constant heat transfer coefficient $h = 30\,\mathrm{W/(m^2{\cdot}K)}$, and the radiation heat transfer between particles and surroundings with emissivity $\varepsilon_{pw} = 0.8$ and surroundings temperature $T_{\mathrm{inf}} = 1200\mathrm{K}$.

Table 1: Proximate and ultimate analysis of Illinois #6 and Guizhou coals.

	Proximate %				Ultimate (daf) %				
	Moisture	Ash	Volatiles	Fixed C	C	H	O	N	S
Illinois #6	9.64	8.00	36.78	45.58	78.51	5.49	9.81	1.36	4.83
Guizhou	5.70	31.80	22.80	39.70	84.00	5.30	7.60	1.60	1.50

3. Temperature criteria for MILD coal combustion

The temperature criteria, shown in (1) and (2), require the inlet temperature, T_{inlet}, and the self-ignition temperature, $T_{\mathrm{self-ignition}}$, which is the lowest temperature at which the fuel-air mixture spontaneously ignites. Since $T_{\mathrm{self-ignition}}$ is a function of T_{inlet} and the composition of the fuel and oxidizer streams, we must identify the composition and temperature of the gas-phase fuel released from the coal particles.

As indicated in §1, the fuel released from the coal particles to gas phase is comprised of water vapor (‘mois’), light gas (‘lg’), products of tar/soot reactions (‘tp’) and products of char oxidation/gasification (‘char-p’), with the relative contributions of each of these varying over time.

From the criterion for MILD that $T_{\mathrm{inlet}} > T_{\mathrm{self-ignition}}$, the reactants need to be hot enough to ignite spontaneously. Thus, we need T_{inlet} and $T_{\mathrm{self-ignition}}$ for the mixture of oxidizer and gas-phase fuel *just before ignition occurs*. Obtaining the ignition delay becomes the first step to get the fuel streams. Following [27], we define ignition delay based on the time when CH reaches 50% of its maximum value. Figure 2 shows the CH mass fraction as well as gas and particle temperatures as functions of residence time. The vertical dashed line indicates the position of ignition with $Y_{\mathrm{CH,ign}} = 0.5 Y_{\mathrm{CH,max}}$. Based upon this ignition criterion, we can define the average temperature and composition of each stream [17] using the reaction rates of each subprocess and particle/gas temperature before ignition.

3.1. Temperature of fuel streams

We define the fuel stream temperature by integrating fuel production rates up to the ignition delay time, t_{ign} as

$$T_{\zeta} = \frac{\sum_{j=1}^{n_{\mathrm{size}}} \int_0^{t_{\mathrm{ign}}} T_{\mathrm{p},j} \dot{m}_{\zeta,j} dt}{\sum_{j=1}^{n_{\mathrm{size}}} \int_0^{t_{\mathrm{ign}}} \dot{m}_{\zeta,j} dt}, \tag{41}$$

where ζ refers to the fuel stream contribution and includes ‘mois’ ($\dot{m}_{\zeta,j} = S_{m_{\mathrm{mois}},j}$), ‘lg’ ($\dot{m}_{\zeta,j} = S_{m_{\mathrm{vol}},j} - S_{m_{\mathrm{char}},j} - S_{m_{\mathrm{gtar}},j}$) and ‘char-p’ ($\dot{m}_{\zeta,j} = S^{\mathrm{oxid}}_{m_{\mathrm{char}},j} + S^{\mathrm{gasif,H_2O}}_{m_{\mathrm{char}},j} + S^{\mathrm{gasif,CO_2}}_{m_{\mathrm{char}},j}$). More details on each of these production rates are provided in

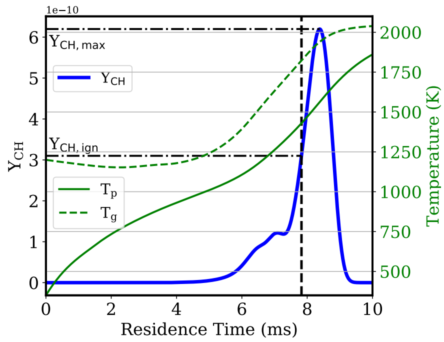

Figure 2: Ignition delay using CH criterion for Illinois #6 coal with model *"$C_{10}H_{10}$+C"* for tar/soot treatment and $T_{\rm oxid}$ = 1200K. The vertical dashed line indicates the ignition delay.

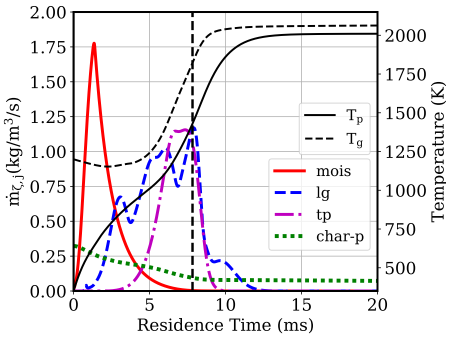

Figure 3: $\dot{m}_{\zeta,\rm j}$ for various fuel streams in (41)-(42) for Illinois #6 coal with model *"$C_{10}H_{10}$+C"* for tar/soot treatment and $T_{\rm oxid}$ = 1200K. The vertical dashed line represents the ignition delay.

§2.2.

If model *"$C_{10}H_{10}$+C"* or *"$C_{10}H_{10}$"* is used for tar/soot treatment, we need to consider the fuel stream from tar/soot reactions ('tp') as well. Tar and soot are assumed to have the same temperature as gas phase in our model. The temperature of tar and soot product ($T_{\rm tp}$) is defined as

$$T_{\rm tp} = \frac{\int_0^{t_{\rm ign}} T_{\rm g}\dot{m}_{\rm tp}dt}{\int_0^{t_{\rm ign}} \dot{m}_{\rm tp}dt}, \tag{42}$$

Here $\dot{m}_{\rm tp}$ represents the net production rate of gas released from tar and soot reactions. For model *"$C_{10}H_{10}$+C"*, $\dot{m}_{\rm tp}$ is the sum of production rate of H_2 from (21a), oxidation rate of tar from (21b) and oxidation rate of soot from (21c). For model *"$C_{10}H_{10}$"*, $\dot{m}_{\rm tp}$ is the sum of the oxidation rates of tar from (22b) and soot from (22c).

Figure 3 shows $\dot{m}_{\zeta,j}$ as a function of residence time for Illinois #6 coal with model *"$C_{10}H_{10}$+C"* for tar/soot treatment as an example. Moisture is vaporized in a short time (≈6ms) and at relatively low particle temperatures, giving lower temperature of the moisture stream as shown in Table 2. Tar/soot reactions start when enough tar is released during devolatilization and accumulates in gas phase. Tar/soot reaction rates reach a maximum value near ignition, resulting in the highest temperature for the tar/soot products stream. The maximum reaction rate of char oxidation/gasification occurs near the inlet prior to ignition, leading to a low temperature for the char products stream.

Table 2: Fuel streams from various subprocesses with model *"$C_{10}H_{10}$+C"* for tar/soot treatment for Illinois #6 coal. Temperature, species mass fraction and mass fractions of each stream in the fuel mixture are given.

Stream	T (K)	Composition (ω_i)								Mass Fraction
		H_2	H_2O	HCN	CO_2	CO	CH_4	O_2	N_2	
mois	714	-	1.0	-	-	-	-	-	-	0.059
lg	1091	0.038	0.135	0.105	0.112	0.382	0.228	-	-	0.097
tp	1541	0.002	0.066	-	-	0.257	-	-	0.675	0.578
char-p	858	-	-	-	0.166	0.151	-	-	0.683	0.266
fuel	1241	0.005	0.110	0.010	0.055	0.226	0.022	-	0.572	1
fuel+oxid	1219	0.002	0.046	0.004	0.023	0.093	0.009	0.137	0.686	-

3.2. *Composition of the fuel stream*

The fuel evolved from the coal particle is comprised of moisture, light gas, products of tar/soot reactions, and products of char gasification/oxidation. Below, we define the composition of each of these streams.

3.2.1. *Moisture stream*

Only H_2O is released from vaporization: $\omega_{H_2O}^{\mathrm{mois}} = 1$.

3.2.2. *Light gas stream*

Given the production rate of the i^{th} species from devolatilization of the j^{th} particle size class, $\dot{m}_i^{\mathrm{lg},j}$ which can be obtained from $S_{m_{gk},j}$ (see §2.2.2), we obtain the average light gas stream composition from

$$\omega_i^{\mathrm{lg}} = \frac{\sum_{j=1}^{n_{\mathrm{size}}} \int_0^{t_{\mathrm{ign}}} \dot{m}_i^{\mathrm{lg},j} dt}{\sum_{j=1}^{n_{\mathrm{size}}} \int_0^{t_{\mathrm{ign}}} \dot{m}^{\mathrm{lg},j} dt}, \tag{43}$$

using the CPD model, which includes $i = \{CH_4, CO, CO_2, H_2, H_2O, NH_3, HCN\}$.

3.2.3. *Tar/soot products stream*

For model *"$C_{10}H_{10}$+C"*, tar/soot products are composed of H_2 from (21a), CO, H_2O and inert components of the oxidizer (N_2 if no flue gas is recirculated) from (21b), and CO and inert components of the oxidizer from (21c). For model *"$C_{10}H_{10}$"*, tar/soot products include CO, H_2O and inert components of the oxidizer from (22b) and (22c). The mass fractions of species are calculated based on the reaction rates of (21) or (22). Using model *"$C_{10}H_{10}$+C"* as an example, the composition of tar/soot products can be calculated by the following process. Using the reaction rates of tar/soot from (21a)-(21c), $S_{m_{\mathrm{tar}}}^{\mathrm{tarToSoot}}$, $S_{m_{\mathrm{tar}}}^{\mathrm{oxid}}$ and $S_{m_{\mathrm{soot}}}^{\mathrm{oxid}}$, the total masses of H_2, CO and H_2O produced from (21), and the mass of O_2 consumed by (21b) and (21c) can be obtained by

$$m_{\mathrm{H_2}}^{\mathrm{tp}} = -\int_0^{t_{\mathrm{ign}}} 5\frac{M_{w,\mathrm{H_2}}}{M_{w,\mathrm{tar}}} S_{m_{\mathrm{tar}}}^{\mathrm{tarToSoot}} dt \tag{44}$$

$$m_{\mathrm{CO}}^{\mathrm{tp}} = -\int_0^{t_{\mathrm{ign}}} \left(10\frac{M_{w,\mathrm{CO}}}{M_{w,\mathrm{tar}}} S_{m_{\mathrm{tar}}}^{\mathrm{oxid}} + \frac{M_{w,\mathrm{CO}}}{M_{w,\mathrm{soot}}} S_{m_{\mathrm{soot}}}^{\mathrm{oxid}}\right) dt \tag{45}$$

$$m_{\mathrm{H_2O}}^{\mathrm{tp}} = -\int_0^{t_{\mathrm{ign}}} 5\frac{M_{w,\mathrm{H_2O}}}{M_{w,\mathrm{tar}}} S_{m_{\mathrm{tar}}}^{\mathrm{oxid}} dt \tag{46}$$

$$m_{\mathrm{O_2}}^{\mathrm{tp}} = \int_0^{t_{\mathrm{ign}}} \left(\frac{15}{2}\frac{M_{w,\mathrm{O_2}}}{M_{w,\mathrm{tar}}} S_{m_{\mathrm{tar}}}^{\mathrm{oxid}} + \frac{1}{2}\frac{M_{w,\mathrm{O_2}}}{M_{w,\mathrm{soot}}} S_{m_{\mathrm{soot}}}^{\mathrm{oxid}}\right) dt \tag{47}$$

Here, M_w is the molecular weight of species. The mass of inert gas (N_2 when there is no dilution) in the fuel stream can be expressed using the consumption of O_2,

$$m_{\mathrm{N_2}}^{\mathrm{tp}} = \frac{Y_{\mathrm{N_2,oxid}}}{Y_{\mathrm{O_2,oxid}}} m_{\mathrm{O_2}}^{\mathrm{tp}}, \tag{48}$$

with $Y_{\mathrm{N_2,oxid}}$ and $Y_{\mathrm{O_2,oxid}}$ denoting the mass fraction of N_2 and O_2 in the oxidizer. The total mass and compositions of fuel stream 'tp' can be expressed

$$m^{\mathrm{tp}} = \sum_i m_i^{\mathrm{tp}}, \tag{49}$$

$$\omega_i^{\mathrm{tp}} = \frac{m_i^{\mathrm{tp}}}{m^{\mathrm{tp}}}, \tag{50}$$

with $i = \{\mathrm{H_2}, \mathrm{CO}, \mathrm{H_2O}, \mathrm{N_2}\}$.

3.2.4. Char products stream

From the char oxidation and gasification schemes, the char product is composed of CO, CO_2 and inert components of oxidizer from char oxidation, CO and inert components of oxidizer from (29), and CO, H_2 and inert components of oxidizer from (30). The composition is calculated based on the reaction rates of char oxidation and gasification, (29) and (30), similar to the method shown in (44)-(50).

Table 2 gives the fuel stream composition in the third column. To get the composition of the light gas stream, the production rates of light gas species $\dot{m}_i^{\mathrm{lg},j}$ are presented in Figure 4. The total production rate of light gases is represented by the black solid line. The area under the black line is divided into six parts by different colors, one for each species. From the CPD parameters of Illinois #6 coal, nitrogen in the volatiles is released as HCN. Therefore, no NH_3 is obtained in the light gas stream. CO and CH_4 have the largest production rates, resulting in the biggest mass fractions of CO and CH_4 as indicated in Table 2. The production of H_2 starts at around 6 ms and has the smallest production rate, resulting in the smallest mass fraction. From Table 2, there is no H_2 in products of char oxidation/gasification. Figure 5 compares the reaction rates of char oxidation and gasification. Char gasification does

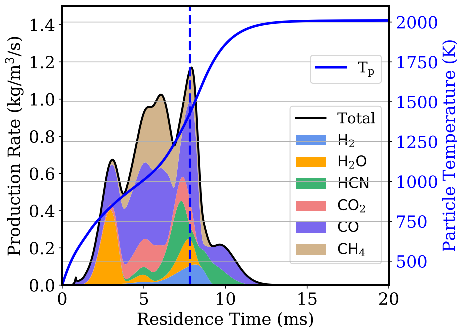

Figure 4: Contributions of light-gas devolatilization rates to the total (black line) for Illinois #6 coal with model *"$C_{10}H_{10}$+C"* for tar/soot treatment and T_{oxid} = 1200K. The vertical dashed line represents the ignition delay.

not start until 2 ms after ignition due to the low concentration of CO_2 and H_2O and low particle temperature before ignition. Therefore, only char oxidation contributes to the char products stream before ignition.

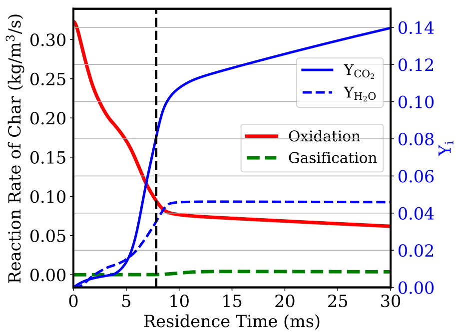

Figure 5: Rates of char oxidation and gasification for Illinois #6 coal with model *"$C_{10}H_{10}$+C"* for tar/soot treatment and T_{oxid} = 1200K. The vertical dashed line represents the ignition delay.

3.3. Fuel mixture and inlet temperature

Once the composition and temperature of the fuel streams are obtained via the procedures outlined in §3.1 and §3.2, we can get the fuel mixture of four streams and the inlet temperature used in the criteria. The fuel mixture is obtained using a mass-weighted average of each stream.

The last column of Table 2 shows the mass fractions of each fuel stream in the fuel mixture. Tar/soot and char products account for nearly 85% of the total mass of fuel mixture due to the inclusion of inert gas from oxidizer in both streams. The tar/soot products not only have the largest mass contribution to the fuel, but they are also produced at the highest temperature, resulting in a high fuel mixture temperature, as shown in Table 2.

The inlet temperature is the mixture temperature of the unreacted fuel and oxidizer at the prescribed equivalence ratio (stoichiometric here). Given the choice of oxidizer temperature of 1200K, we obtain T_{inlet} = 1219K in this case (see Table 2).

3.4. Self-ignition temperature

Another important parameter in the criteria is the self-ignition temperature of the fuel-oxidizer mixture, which has the compositions shown in the last row of Table 2. The self-ignition temperature, $T_{\mathrm{self-ignition}}$, is identified by running a constant-pressure, adiabatic perfectly stirred reactor with residence time of 10s parametrically over initial temperatures using composition of fuel-oxidizer mixture until the ignition point is identified. Figure 6 shows results for this procedure for Illinois #6 coal with model *"$C_{10}H_{10}$+C"* for tar/soot treatment, and indicates a self-ignition temperature of approximately 760K. The inlet temperature obtained in §3.3, 1291K, is higher than the self-ignition temperature here, indicating that criterion (1) is satisfied.

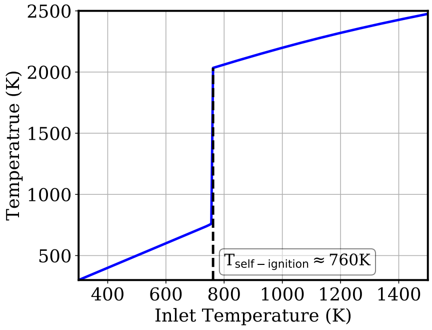

Figure 6: Steady state temperatures of reactant mixture under various inlet temperatures in perfectly-stirred reactor. The reactant mixture comes from Illinois #6 coal combustion with model *"$C_{10}H_{10}$+C"* for tar/soot treatment and T_{oxid} = 1200K.

4. Application of temperature criteria to MILD coal combustion

In this section, the method proposed in §3 is applied to coal combustion to demonstrate its use in determining limits for the MILD combustion regime. The effects of tar/soot treatment, coal types and oxidizer temperature on the achievement of MILD coal combustion are discussed.

MILD combustion occurs in a volumetric region where reactants are highly diluted by recirculated flue gas through internal or external recirculation. The recirculated flue gas can preheat and dilute the reactants before ignition, which is the most important step to reach MILD regime. To quantify the dilution degree of reactants in MILD combustion, Wunning, *et al.* [38] define the dilution rate (K_v) as

$$K_v = \frac{\dot{m}_e}{\dot{m}_o + \dot{m}_f}, \tag{51}$$

where $\dot{m}_e$, $\dot{m}_o$ and $\dot{m}_f$ are the mass flow rates of entrained flue gas, initial oxidizer and initial fuel respectively. Four dilution rates, K_v = 0.5, 1.0, 1.5 and 2.0, are considered here to identify the dilution rate required to achieve MILD coal combustion. The combustion products from the reactor with K_v = 0 (giving a temperature around 1500K) are used as recirculated flue gas in this work. When K_v > 0, the pure oxidizer is mixed with the recirculated flue gas before being introduced to the rector, with the mass of recirculated flue gas $\dot{m}_e$ calculated from (51). The inlet velocity and particle Reynolds number are calculated using the mass flow rate of the new oxidizer $\dot{m}_e + \dot{m}_o$.

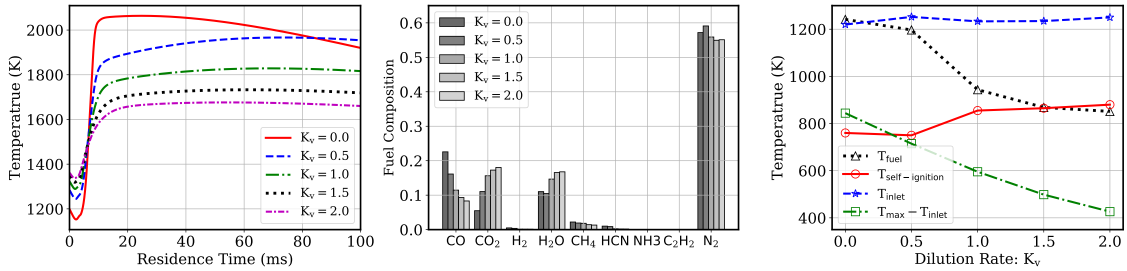

(a) Gas temperature T_g (b) Fuel mixture composition ω_{fuel} (c) MILD criteria indicators.

Figure 7: Comparison of gas temperature, fuel composition and combustion regime classification under different dilution rates K_v for Illinois #6 coal with model *"$C_{10}H_{10}$+C"* for tar/soot treatment and T_{oxid} = 1200K.

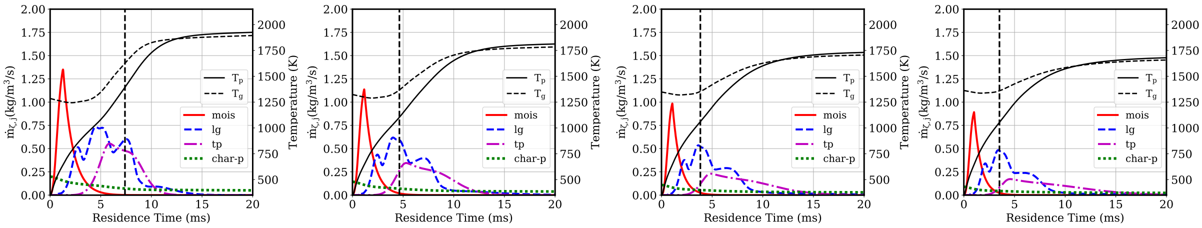

(a) K_v = 0.5 (b) K_v = 1.0 (c) K_v = 1.5 (d) K_v = 2.0

Figure 8: $\dot{m}_{\zeta,j}$ for various fuel streams in (41)-(42) under different dilution rates K_v for Illinois #6 coal with model *"$C_{10}H_{10}$+C"* for tar/soot treatment and T_{oxid} = 1200K. The vertical dashed line represents the ignition delay.

4.1. Achievement of MILD coal combustion by recirculation of flue gas

The required dilution rate to reach MILD regime for Illinois #6 coal with model *"$C_{10}H_{10}$+C"* for tar/soot treatment and undiluted oxidizer at 1200K is evaluated in this section. Figure 7 compares the gas temperature in the reactor, fuel composition and combustion regime classification under various K_v. As K_v increases, the reactor inlet temperature increases while the maximum temperature decreases as shown in Figure 7a. This leads to a more uniform temperature field in the reactor, as is necessary for MILD combustion. The composition of fuel streams for various K_v are compared in Figure 7b. Mass fractions of CO_2 and H_2O increase with K_v due to the recirculated flue gas in oxidizer, which mainly includes CO_2 and H_2O. Given the high heat capacity of CO_2, higher $T_{\text{self-ignition}}$ is observed for large K_v as indicated in Figure 7c. The mass fraction of CO (which has contributions from light gas, tar/soot and char oxidation/gasification) decreases with K_v. As shown in Figure 8, the ignition delay decreases due to the high temperature of oxidizer as K_v increases. However, the varying trends of the released rates for each stream $\dot{m}_{\zeta,j}$ are similar for various K_v. Also, the shift in the time when tar/soot products start to release is not as substantial as the shift in the ignition delay as K_v increases. The combining effects of above three factors yield less tar/soot products in the fuel mixture and a smaller mass fraction of CO.

Figure 7c compares three temperatures used in the temperature criteria for MILD combustion (1) and (2), including T_{inlet}, $T_{\text{self-ignition}}$ and $(T_{\max} - T_{\text{inlet}})$. The fuel stream temperature (defined in §3.1) is also shown for reference. The inlet temperature is affected by fuel and oxidizer temperatures. When K_v increases from 0 to 2.0, oxidizer temperature increases (indicated by temperatures at zero residence time in Figure 7a), while the fuel temperature decreases due to the decrease of the maximum gas temperature as shown in Figure 7a and the decrease of ignition delay as shown in Figure 8. Another factor affecting T_{inlet} is the mass ratio of oxidizer and fuel under the same equivalence ratio. When $K_v > 0$, more flue gases are included in the oxidizer, resulting in an increase of oxidizer-to-fuel mass ratio. Thus, the large decrease of fuel temperature ($\approx$ 400K) is balanced by the small increase of oxidizer temperature ($\approx$ 160K) and the increase of oxidizer-to-fuel ratio. Almost constant T_{inlet} is obtained for various K_v. The first MILD criterion, $T_{\text{inlet}} > T_{\text{self-ignition}}$, is satisfied for all K_v. The second MILD criterion, $(T_{\max} - T_{\text{inlet}}) < T_{\text{self-ignition}}$, is obtained when $K_v \geq 0.5$. That is, MILD coal combustion is achieved when $K_v \geq 0.5$ for Illinois #6 coal with undiluted oxidizer at 1200K.

4.2. Impacts of tar/soot treatment

From the above analysis, we observed that the tar/soot products account for most of the fuel stream mixture when model "$C_{10}H_{10}$+C" is used for tar/soot treatment as shown in Table 2. We now consider the effect of various tar/soot treatments on the characterization of MILD combustion for Illinois #6 coal with undiluted oxidizer at 1200K.

Figure 9 compares the temperatures of fuel streams and gas temperatures using various tar/soot treatments with different K_v values. Figure 9a shows that, when either model "$C_{10}H_{10}$+C" or "$C_{10}H_{10}$" is used, the temperatures of light gas and tar/soot products are the same. High temperature of 'tp' results in high fuel temperature T_{fuel} under all K_v for model "$C_{10}H_{10}$+C" and "$C_{10}H_{10}$" than "C_2H_2" shown in Figure 9b. The decrease of ignition delay with K_v and lower gas temperature before ignition for big K_v as shown in Figure 9c and 9d give lower temperature of fuel streams and fuel mixture as indicated in Figure 9a and 9b. (The gas temperature of model "$C_{10}H_{10}$" is not shown here, because it gives similar results to model "$C_{10}H_{10}$+C"). Comparing tar/soot reaction schemes (21) and (22) for models "$C_{10}H_{10}$+C" and "$C_{10}H_{10}$", all H in tar is oxidized to H_2O in model "$C_{10}H_{10}$", while part of H is released as H_2 in model "$C_{10}H_{10}$+C", resulting in more oxidizer required for model "$C_{10}H_{10}$". Thus, more inert species in oxidizer with high oxidizer temperature, especially for cases $K_v \neq 0$, gives higher $T_{\text{fuel}}^{\mathrm{C_{10}H_{10}}}$ than $T_{\text{fuel}}^{\mathrm{C_{10}H_{10}+C}}$.

Figure 10 shows the inlet temperature, self-ignition temperature, and the temperature rise in the reactor as a function of the dilution rate, K_v, for each of the three tar/soot treatments. We see that the difference of T_{inlet} among three models decreases with K_v. With the increase of K_v, more hot products are mixed with oxidizer, giving high temperature for oxidizer. The big difference among T_{fuel} shown in Figure 9b is balanced by the bigger amount of hot products in oxidizer, resulting in almost the same T_{inlet} for $K_v = 2.0$. The first MILD criterion, $T_{\text{inlet}} > T_{\text{self-ignition}}$, is satisfied for all cases. The second MILD criterion, $(T_{\max} - T_{\text{inlet}}) < T_{\text{self-ignition}}$, is achieved when $K_v \geq 0.5$ for

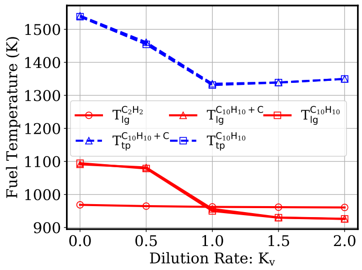

(a) T_{lg} and T_{tp}

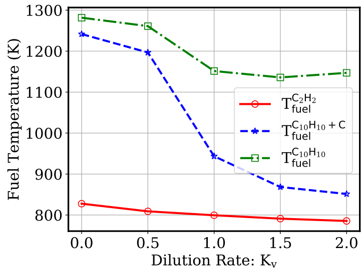

(b) Fuel mixture temperature T_{fuel}

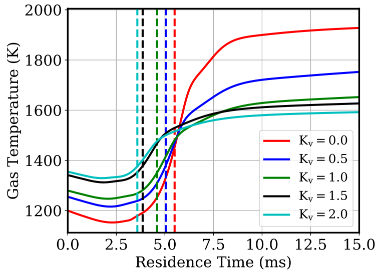

(c) Gas temperature (“C_2H_2”)

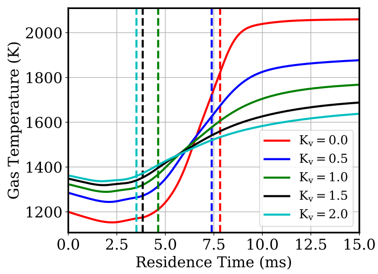

(d) Gas temperature (“$C_{10}H_{10}$+C”)

Figure 9: Comparison of fuel temperature and gas temperature with different tar/soot treatments and T_{oxid} = 1200K for Illinois #6 coal. The vertical dashed lines in Figure 9c and 9d indicate the ignition delay corresponding to gas phase temperature with the same color in the figure.

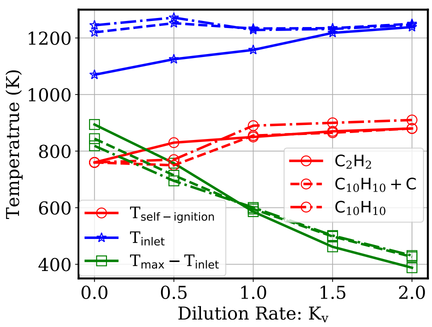

Figure 10: Comparison of combustion regime classification with different tar/soot treatments and T_{oxid} = 1200K for Illinois #6 coal.

Table 3: Fuel streams from various subprocesses with model *"$C_{10}H_{10}$+C"* for tar/soot treatment for Guizhou coal. Temperature, species mass fraction and mass fractions of each stream in the fuel mixture are given.

Stream	T (K)	Composition (ω_i)								Mass Fraction
		H_2	H_2O	HCN	NH_3	CO_2	CO	CH_4	N_2	
mois	676	-	1.0	-	-	-	-	-	-	0.054
lg	1070	0.033	0.178	0.081	0.001	0.176	0.341	0.190	-	0.094
tp	1447	0.001	0.073	-	-	-	0.247	-	0.679	0.495
char-p	895	-	-	-	-	0.156	0.163	-	0.681	0.357

all three tar/soot treatments. Model *"C_2H_2"* gives reasonable prediction of the required K_v to reach MILD regime, even $T_{\text{self-ignition}}$, T_{inlet} and $(T_{\max} - T_{\text{inlet}})$ show little change from the other two models. This is encouraging as model *"C_2H_2"* is much simpler to implement.

4.3. Impact of coal type

Different ranks of coal give different amounts of volatiles and fixed carbon in the particles, which have significant effects on the composition and temperatures of fuel stream. The effects of coal type on the achievement of MILD coal combustion is studied in this section by comparing the results using Guizhou coal with the aforementioned results for Illinois #6 coal. Figure 11 gives the change of $\dot{m}_{\zeta,j}$ with residence time for Guizhou coal with model *"$C_{10}H_{10}$+C"* for tar/soot treatment. Comparing Figure 11 with Figure 3, smaller $\dot{m}_{\text{lg},j}$ and $\dot{m}_{\text{tp},j}$ are obtained due to less volatiles in

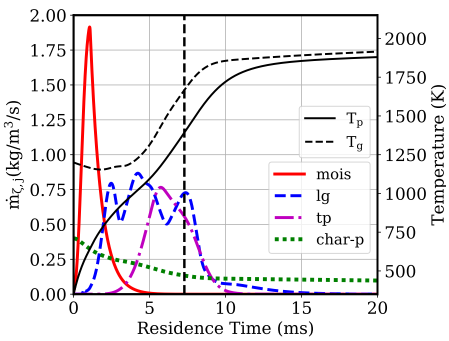

Figure 11: $\dot{m}_{\zeta,j}$ for various fuel streams in (41)-(42) with model *"$C_{10}H_{10}$+C"* for tar/soot treatment, K_v = 0.0 and T_{oxid} = 1200K for Guizhou coal. The vertical dashed line represents the ignition delay time.

Guizhou coal than Illinois #6 coal. The gas/particle heat up rates are smaller for Guizhou coal than that for Illinois #6 coal, causing lower temperature of volatiles as well as the tar/soot products, as shown in Table 3. The compositions of each fuel stream for Guizhou and Illinois #6 coal are similar, giving similar $T_{\text{self-ignition}}$ for two coal types in Figure 12b.

Figures 12a shows the comparison of fuel temperature for various values of K_v between Illinois #6 and Guizhou coal types. The fuel temperature for Guizhou coal is a little lower than that for Illinois #6 coal due to the lower gas/particle temperature shown in Figure 11. This gives lower inlet temperature T_{inlet} for Guizhou coal as shown in Figure 12b. MILD combustion is achieved when $K_v \geq 0.5$ for Guizhou coal, the same as Illinois #6 coal. The

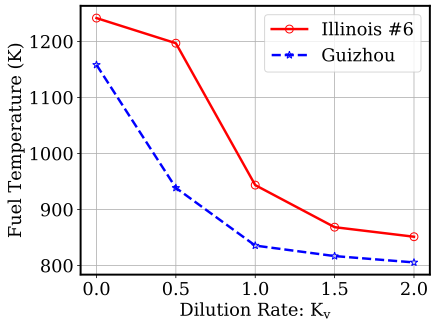

(a) Fuel mixture temperature T_{fuel}

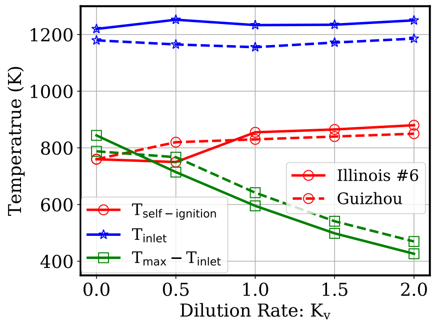

(b) Combustion regime classification

Figure 12: Comparison of fuel temperature and combustion regime classification with "$C_{10}H_{10}$+C" for tar/soot treatment and T_{oxid} = 1200K between Illinois #6 and Guizhou coal types.

difference of volatile and fixed carbon contents in two coal types does not have big effects on the achievement of MILD coal combustion.

4.4. Impacts of oxidizer temperature

MILD combustion can be achieved without preheating the oxidizer when the dilution rate of flue gas is big enough [5, 39, 40]. In this section, the effects of oxidizer temperature on the achievement of MILD coal combustion is studied.

Figure 13 gives $\dot{m}_{\zeta,j}$ and gas/particle temperatures as a function of residence time for Illinois #6 coal with T_{oxid} = 350K[1]. Compared with Figure 3, the ignition delay is approximately 9 times longer when using lower oxidizer temperature. The maximum temperature decreases, which is helpful to get MILD combustion. Additionally, ignition is more pronounced for the lower oxidizer temperature, resulting in fuel being released within a short time when ignition occurs. The release rates of fuel from volatiles and tar/soot are small before ignition due to low gas/particle temperatures. This gives lower temperatures of all fuel streams and fuel mixture as compared in Figure 14 and lower inlet temperature as shown in Figure 15. As discussed in [31], the fitted activation energies are unusually low for the

[1]Note that for lower oxidizer feed temperatures, ignition is achieved via internal heat transfer within the reactor (T_{inf} = 1200K), as described in §2.4.

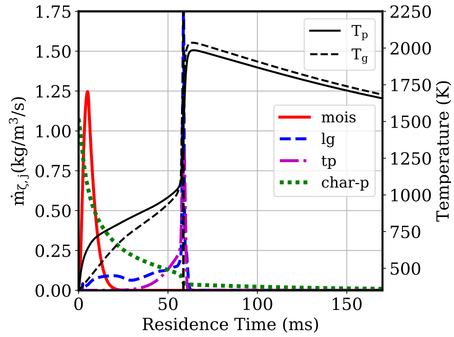

Figure 13: $\dot{m}_{\zeta,j}$ for various fuel streams in (41)-(42) with model *"$C_{10}H_{10}$+C"* for tar/soot treatment, K_v = 0.0 and T_{oxid} = 350K for Illinois #6 coal. The vertical black dashed line represents the position of the ignition.

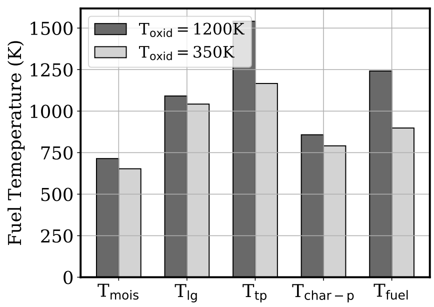

Figure 14: Temperatures of fuel stream for Illinois #6 coal with *"$C_{10}H_{10}$+C"* for tar/soot treatment K_v = 0.0 under various oxidizer temperatures.

char oxidation reaction for the coals considered. Consequently, char oxidation is predicted to occur at low temperatures (<500K) and is the reason computations predict that the particle temperature is higher than the gas temperature prior to ignition.

Figure 15 shows the achievement of MILD coal combustion using various K_v under two oxidizer temperatures. When K_v = 0.0, both criteria (1) and (2) are not satisfied with $T_{\text{inlet}} < T_{\text{self-ignition}}$ and $T_{\max} - T_{\text{inlet}} > T_{\text{self-ignition}}$. T_{inlet} increases and $T_{\max} - T_{\text{inlet}}$ decreases with K_v for T_{oxid} = 350K. When $K_v \geq 1.0$, MILD coal combustion is achieved by satisfying criteria (1) and (2) for case with T_{oxid} = 350K. Comparing with results with T_{oxid} = 1200K, the required dilution rate K_v increases from 0.5 to 1 when using lower oxidizer temperature 350K.

5. Conclusions

Temperature criteria, $T_{\text{inlet}} > T_{\text{self-ignition}}$ and $(T_{\max} - T_{\text{inlet}}) < T_{\text{self-ignition}}$, are widely applied to help classify the MILD combustion from traditional combustion. Unfortunately, T_{inlet} and $T_{\text{self-ignition}}$ are not actually measured or compared to these MILD combustion criteria in previous studies of MILD coal combustion. In this work, we propose a method to obtain the gas-phase fuel mixture, including streams from moisture vaporization, devolatilization, tar/soot reactions and char oxidation/gasification reactions in coal combustion. The mixture of the gas-phase fuel and oxidizer is used to get T_{inlet} and $T_{\text{self-ignition}}$ used in the MILD combustion criteria. The comparison of three tar/soot treatments

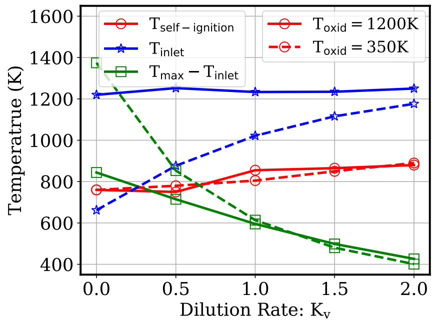

Figure 15: Comparison of combustion regime classifications for Illinois #6 coal with "$C_{10}H_{10}$+C" for tar/soot treatment under various oxidizer temperatures.

have been made by assuming tar is C_2H_2 without considering soot, assuming tar is $C_{10}H_{10}$ and soot is carbon, and assuming both tar and soot $C_{10}H_{10}$. These three treatments give essentially the same classification of MILD combustion. The comparison between Illinois #6 and Guizhou coals indicated that temperature and compositions of fuel streams are affected by the rank of the coal, which may alert the MILD coal combustion regime. Both inlet and maximum temperature in the reactor decreases when using lower temperature for oxidizer. The required dilution rate increases for lower oxidizer temperature.

Acknowledgments

This research was funded by the National Science Foundation under grant NSF1704141.

Appendix A. Derivation of Governing Equations for the Idealized PFR Model

Appendix A.1. Governing Equations of Gas Phase

The general governing equations of gas phase is given as

$$\frac{\partial \rho_g}{\partial t} = -\frac{\partial \rho_g u}{\partial x} + S_{m_g} \tag{A.1}$$

$$\frac{\partial \rho_g u}{\partial t} = -\frac{\partial \rho_g u u}{\partial x} - \frac{\partial p}{\partial x} \tag{A.2}$$

$$\frac{\partial \rho_g Y_i}{\partial t} = -\frac{\partial \rho_g u Y_i}{\partial x} + \omega_i + S_{Y_i} \tag{A.3}$$

$$\frac{\partial \rho_g h_g}{\partial t} = -\frac{\partial \rho_g u h_g}{\partial x} + Q_g + S_{h_g} + \frac{dp}{dt} \tag{A.4}$$

To write the governing equations in weak form, we use chain rule to (A.2)-(A.4). Here we use (A.2) as an example.

$$\rho_g \frac{\partial u}{\partial t} + u \frac{\partial \rho_g}{\partial t} = -\rho_g u \frac{\partial u}{\partial x} - u \frac{\partial \rho_g u}{\partial x} - \frac{\partial p}{\partial x}$$

Substituting (A.1) into above equation:

$$\rho_g \frac{\partial u}{\partial t} + u \left(-\frac{\partial \rho_g u}{\partial x} + S_{m_g} \right) = -\rho_g u \frac{\partial u}{\partial x} - u \frac{\partial \rho_g u}{\partial x} - \frac{\partial p}{\partial x}$$

$$\rho_g \frac{\partial u}{\partial t} + u S_{m_g} = -\rho_g u \frac{\partial u}{\partial x} - \frac{\partial p}{\partial x}$$

$$\frac{\partial u}{\partial t} = -u \frac{\partial u}{\partial x} - \frac{1}{\rho_g} \frac{\partial p}{\partial x} - \frac{u S_{m_g}}{\rho_g} \tag{A.5}$$

Similar for (A.3) and (A.4), we get the weak form of governing equations for gas-phase:

$$\frac{\partial \rho_g}{\partial t} = -\frac{\partial \rho_g u}{\partial x} + S_{m_g} \tag{A.1}$$

$$\frac{\partial u}{\partial t} = -u \frac{\partial u}{\partial x} - \frac{1}{\rho_g} \frac{\partial p}{\partial x} - \frac{u S_{m_g}}{\rho_g} \tag{A.5}$$

$$\frac{\partial Y_i}{\partial t} = -u \frac{\partial Y_i}{\partial x} + \frac{\omega_i + S_{Y_i} - Y_i S_{m_g}}{\rho_g} \tag{A.6}$$

$$\frac{\partial h_g}{\partial t} = -u \frac{\partial h_g}{\partial x} + \frac{Q_g + S_{h_g} - h_g S_{m_g} + \frac{dp}{dt}}{\rho_g} \tag{A.7}$$

Under steady state, we have all LHSs equalling to zero:

$$\frac{d\rho_g u}{dx} = S_{m_g} \tag{A.8}$$

$$\frac{du}{dx} = -\frac{1}{\rho_g u}\frac{dp}{dx} - \frac{S_{m_g}}{\rho_g} \tag{A.9}$$

$$\frac{dY_i}{dx} = \frac{\omega_i + S_{Y_i} - Y_i S_{m_g}}{\rho_g u} \tag{A.10}$$

$$\frac{dh_g}{dx} = \frac{Q_g + S_{h_g} - h_g S_{m_g}}{\rho_g u} + \frac{\frac{dp}{dx}}{\rho_g} \tag{A.11}$$

Using chain rule to the LHS of continuity equation (A.8):

$$u\frac{d\rho_g}{dx} + \rho_g\frac{du}{dx} = S_{m_g}$$

Substitute (A.9) into above equation:

$$u\frac{d\rho_g}{dx} + \rho_g\left(-\frac{1}{\rho_g u}\frac{dp}{dx} - \frac{S_{m_g}}{\rho_g}\right) = S_{m_g}$$

$$\frac{d\rho_g}{dx} = \frac{1}{u^2}\frac{dp}{dx} + \frac{2S_{m_g}}{u} \tag{A.12}$$

For term $\frac{dp}{dx}$, we use ideal gas law $p = \frac{\rho_g R T_g}{M_w}$:

$$\frac{dp}{dx} = \frac{RT_g}{M_w}\frac{d\rho_g}{dx} + \frac{\rho_g R}{M_w}\frac{dT_g}{dx} - \frac{\rho_g R T_g}{M_w^2}\frac{dM_w}{dx} \tag{A.13}$$

For $\frac{dT_g}{dx}$, we have

$$dh_g = C_{p,g} dT_g + \sum_{i=1}^{n_s-1}(h_i - h_{n_s})dY_i$$

$$\frac{dT_g}{dx} = \frac{1}{C_{p,g}}\left(\frac{dh_g}{dx} - \sum_{n=1}^{n_s-1}(h_i - h_{n_s})\frac{dY_i}{dx}\right) \tag{A.14}$$

For $\frac{dM_w}{dx}$, we have

$$M_w = \frac{1}{\sum_{i=1}^{n_s}\frac{Y_i}{M_{w,i}}}$$

$$\frac{dM_w}{dx} = -M_w^2\sum_{i=1}^{n_s-1}\left(\frac{1}{M_{w,i}} - \frac{1}{M_{w,n_s}}\right)\frac{dY_i}{dx} \tag{A.15}$$

Here, h_i and $M_{w,i}$ are the specific enthalpy and molecular weight of i^{th} species.

Substitute (A.10), (A.11), (A.12), (A.14) and (A.15) to (A.13):

$$\frac{dp}{dx} = \Bigg(\frac{2S_{m_g}T_g}{u} + \frac{Q_g + S_{h_g} - h_g S_{m_g}}{uC_{p,g}} \\ - \sum_{i=1}^{n_s-1}\Bigg(\frac{\rho_g}{C_{p,g}}(h_i - h_{n_s}) - \rho_g M_w T_g(\frac{1}{M_{w,i}} - \frac{1}{M_{w,n_s}})\Bigg) \\ \Bigg(\frac{\omega_i + S_{Y_i} - Y_i S_{m_g}}{\rho_g u}\Bigg)\Bigg) / \Bigg(\frac{M_w}{R} - \frac{T_g}{u^2} - \frac{1}{C_{p,g}}\Bigg) \tag{A.16}$$

In summary, the governing equations for gas phase are

$$\frac{d\rho_g}{dx} = \frac{1}{u^2}\frac{dp}{dx} + \frac{2S_{m_g}}{u} \tag{A.12}$$

$$\frac{du}{dx} = -\frac{1}{\rho_g u}\frac{dp}{dx} - \frac{S_{m_g}}{\rho_g} \tag{A.9}$$

$$\frac{dY_i}{dx} = \frac{\omega_i + S_{Y_i} - Y_i S_{m_g}}{\rho_g u} \tag{A.10}$$

$$\frac{dh_g}{dx} = \frac{Q_g + S_{h_g} - h_g S_{m_g}}{\rho_g u} + \frac{\frac{dp}{dx}}{\rho_g} \tag{A.11}$$

where $\frac{dp}{dx}$ is calculated by Eqn. (A.16).

Appendix A.2. Governing Equations of Particle Phase

Particles are considered as a continuous phase in our model. we define the number of particle, total mass of particles, and enthalpy of particles with j^{th} size per *gas* mass as:

$$n_{p,j} = \frac{N_{p,j}}{\rho V} \tag{A.17}$$

$$Y_{p,j} = \frac{m_{p,j}}{\rho V} \tag{A.18}$$

$$h_{p,j} = \frac{H_{p,j}}{\rho V} \tag{A.19}$$

where $N_{p,j}$, $m_{p,j}$ and $H_{p,j}$ representing the total number, mass and enthalpy of particles with j^{th} size. The definitions are similar to the definition of species mass fraction $Y_i = m_i/(\rho_g V)$ with m_i denoting the total mass of i^{th} species. Thus, the governing equations for $n_{p,j}$, $Y_{p,j}$ and $h_{p,j}$ have the same format as (A.10): $\frac{d\phi}{dx} = \frac{S_\phi - \phi S_{m_g}}{\rho_g u}$ with ϕ including $n_{p,j}$, $Y_{p,j}$ and $h_{p,j}$. For $n_{p,j}$, $S_\phi = 0$ is the source term for $N_{p,j}$. For $Y_{p,j}$, $S_\phi = S_{m_p,j}$ is the source term for total mass of particles as shown in (39). For $h_{p,j}$, $S_\phi = S^{\text{total}}_{h_p,j}$ is the total source term for particle enthalpy $H_{p,j}$, including the enthalpy change from heat transfer $Q_{p,j}$ as shown in (12), from the mass loss of particles $S^{\text{mass-loss}}_{h_p,j}$ and from reaction heat of vaporization and char oxidation/gasification $S_{h_p,j}$ as shown in (40). This gives the following equations for $n_{p,j}$,

$Y_{p,j}$ and $h_{p,j}$:

$$\frac{dn_{p,j}}{dx} = -\frac{n_{p,j} S_{m_g}}{\rho_g u} \tag{A.20}$$

$$\frac{dY_{p,j}}{dx} = \frac{S_{m_{p,j}} - Y_{p,j} S_{m_g}}{\rho_g u} \tag{A.21}$$

$$\frac{dh_{p,j}}{dx} = \frac{Q_{p,j} + S^{\text{mass-loss}}_{h_p,j} + S_{h_p,j} - Y_{p,j} S_{m_g}}{\rho_g u} \tag{A.22}$$

For (A.22), we have

$$dh_{p,j} = Y_{p,j} C_{p,p,j} dT_{p,j} + \sum_{\text{CoalComp}} h_{\text{CoalComp},j} dY_{\text{CoalComp},j}$$

$$\frac{dT_{p,j}}{dx} = \frac{1}{Y_{p,j} C_{p,p,j}} \frac{dh_{p,j}}{dx} - \sum_{\text{CoalComp}} \frac{h_{\text{CoalComp},j}}{Y_{p,j} C_{p,p,j}} \frac{dY_{\text{CoalComp},j}}{dx} \tag{A.23}$$

Here 'CoalComp' includes 'mois' for moisture, 'vol' for volatile, 'char' for char and 'ash' for ash. Governing equations of $\frac{dY_{\text{CoalComp},j}}{dx} = \frac{S_{m_{\text{CoalComp}},j} - Y_{\text{CoalComp},j} S_{m_g}}{\rho_g u}$ has the same format as (A.21). Substituting this and (A.22) into (A.23)

$$\begin{aligned}
\frac{dT_{p,j}}{dx} &= \frac{Q_{p,j} + S^{\text{mass-loss}}_{h_p,j} + S_{h_p,j} - Y_{p,j} S_{m_g}}{\rho_g u Y_{p,j} C_{p,p,j}} \\
&\quad - \sum_{\text{CoalComp}} \frac{h_{\text{CoalComp},j}}{Y_{p,j} C_{p,p,j}} \frac{S_{m_{\text{CoalComp}},j} - Y_{\text{CoalComp},j} S_{m_g}}{\rho_g u} \\
&= \frac{1}{\rho_g u Y_{p,j} C_{p,p,j}} \Big(Q_{p,j} + S_{h_p,j} \\
&\quad + (S^{\text{mass-loss}}_{h_p,j} - \sum_{\text{CoalComp}} h_{\text{CoalComp},j} S_{m_{\text{CoalComp}},j}) \\
&\quad - (Y_{p,j} - \sum_{\text{CoalComp}} Y_{\text{CoalComp},j}) S_{m_g} \Big) \\
&= \frac{Q_{p,j} + S_{h_{p,j}}}{\rho_g u Y_{p,j} C_{p,p,j}}
\end{aligned} \tag{A.24}$$

In summary, the governing equations for particles are

$$\frac{dn_{p,j}}{dx} = -\frac{n_{p,j} S_{m_g}}{\rho_g u} \tag{A.20}$$

$$\frac{dY_{p,j}}{dx} = \frac{S_{m_{p,j}} - Y_{p,j} S_{m_g}}{\rho_g u} \tag{A.21}$$

$$\frac{dT_{p,j}}{dx} = \frac{Q_{p,j} + S_{h_{p,j}}}{\rho_g u Y_{p,j} C_{p,p,j}} \tag{A.24}$$

References

[1] A. Cavaliere, M. De Joannon, Mild combustion, Prog. Energy Combust. Sci. 30 (2004) 329–366.

[2] J. P. Kim, U. Schnell, G. Scheffknecht, A. C. Benim, Numerical modelling of MILD combustion for coal, Progress in Computational Fluid Dynamics 7 (2007) 337–346.

[3] P. F. Li, J. C. Mi, B. B. Dally, F. F. Wang, L. Wang, Z. H. Liu, S. Chen, C. G. Zheng, Progress and recent trend in MILD combustion, Science China Technological Sciences 54 (2011) 255–269.

[4] M. Noor, A. P. Wandel, T. Yusaf, Design and Development of MILD Combustion Burner, Journal of Mechanical Engineering and Sciences 5 (2014) 662–676.

[5] M. Saha, B. B. Dally, P. R. Medwell, E. Cleary, An Experimental Study of MILD Combustion of Pulverized Coal in a Recuperative Furnace, Korean Combustion Society, Gyeongju, Korea, 2013.

[6] M. Saha, B. B. Dally, P. R. Medwell, E. M. Cleary, Moderate or Intense Low oxygen Dilution (MILD) combustion characteristics of pulverized coal in a self-recuperative furnace, Energy & Fuels 28 (2014) 6046–6057.

[7] P. Li, F. Wang, Y. Tu, Z. Mei, J. Zhang, Y. Zheng, H. Liu, Z. Liu, J. Mi, C. Zheng, Moderate or intense low-oxygen dilution oxy-combustion characteristics of light oil and pulverized coal in a pilot-scale furnace, Energy and Fuels 28 (2014) 1524–1535.

[8] M. Weidmann, D. Honoré, V. Verbaere, G. Boutin, S. Grathwohl, G. Godard, C. Gobin, R. Kneer, G. Scheffknecht, Experimental characterization of pulverized coal MILD flameless combustion from detailed measurements in a pilot-scale facility, Combustion and Flame 168 (2016) 365–377.

[9] Z. Mao, L. Zhang, X. Zhu, D. Zhou, W. Liu, C. Zheng, Investigation on coal moderate or intense low-oxygen dilution combustion with high-velocity jet at pilot-scale furnace, Applied Thermal Engineering 111 (2017) 387–396.

[10] M. Vascellari, H. Xu, C. Hasse, Flamelet modeling of coal particle ignition, Proceedings of the Combustion Institute 34 (2013) 2445–2452.

[11] J. Watanabe, K. Yamamoto, Flamelet model for pulverized coal combustion, Proceedings of the Combustion Institute 35 (2015) 2315–2322.

[12] J. Watanabe, T. Okazaki, K. Yamamoto, K. Kuramashi, A. Baba, Large-eddy simulation of pulverized coal combustion using flamelet model, Proceedings of the Combustion Institute 36 (2017) 2155–2163.

[13] M. Rieth, A. G. Clements, M. Rabaçal, F. Proch, O. T. Stein, A. M. Kempf, Flamelet LES modeling of coal combustion with detailed devolatilization by directly coupled CPD, Proceedings of the Combustion Institute 36 (2017) 2181–2189.

[14] M. Rieth, A. M. Kempf, O. T. Stein, A. Kronenburg, C. Hasse, M. Vascellari, Evaluation of a flamelet/progress variable approach for pulverized coal combustion in a turbulent mixing layer, Proceedings of the Combustion Institute 37 (2019) 2927–2934.

[15] X. Wen, H. Wang, Y. Luo, K. Luo, J. Fan, Evaluation of flamelet/progress variable model for laminar pulverized coal combustion, Physics of Fluids 29 (2017).

[16] X. Wen, Y. Luo, K. Luo, H. Jin, J. Fan, LES of pulverized coal combustion with a multi-regime flamelet model, Fuel 188 (2017) 661–671.

[17] J. McConnell, J. C. Sutherland, Assessment of various tar and soot treatment methods and a priori analysis of the steady laminar flamelet model for use in coal combustion simulation, Fuel 265 (2020) 116775.

[18] M. Saha, B. B. Dally, A. Chinnici, P. R. Medwell, Effect of co-flow oxygen concentration on the MILD combustion of pulverised coal, Fuel Processing Technology 193 (2019) 7–18.

[19] W. Eisermann, P. Johnson, W. L. Conger, Estimating thermodynamic properties of coal, char, tar and ash, Fuel Processing Technology 3 (1980) 39–53.

[20] R. A. MacDonald, J. E. Callanan, K. M. McDermott, Heat Capacity of a Medium-Volatile Bituminous Premium Coal from 300 to 520 K. Comparison with a High-Volatile Bituminous Nonpremium Coal, Energy and Fuels 1 (1987) 535–540.

[21] T. K. Bergman, A. S. Lavine, F. P. Incropera, D. P. Dewitt, Intorduction to heat transfer, John Wiley & Sons, Inc., fourth edition, 2002.

[22] G. Nellis, S. Klein, Heat Transfer, Cambridge University Press, Cambridge, 2008.

[23] T. H. Fletcher, A. R. Kerstein, R. J. Pugmire, M. Solum, D. M. Grant, A Chemical Percolation Model For Devolatilization: Summary, Technical Report, Combustion Research Facility, Sandia National Laboratories, 1992.

[24] R. Jupudi, V. Zamansky, T. Fletcher, Prediction of light gas composition in coal devolatilization, Energy & Fuels 23 (2009) 3063–3067.

[25] T. Fletcher, Soot in coal combustion systems, Progress in Energy and Combustion Science 23 (2002) 283–301.

[26] A. Cuoci, T. Faravelli, S. Ferrario, C. Saggese, J. Camacho, A. Frassoldati, E. Ranzi, H. Wang, Kinetic modeling of particle size distribution of soot in a premixed burner-stabilized stagnation ethylene flame, Combustion and Flame 162 (2015) 3356–3369.

[27] B. Goshayeshi, J. C. Sutherland, A comparison of various models in predicting ignition delay in single-particle coal combustion, Combustion and Flame 161 (2014) 1900–1910.

[28] B. Goshayeshi, J. C. Sutherland, Prediction of oxy-coal flame stand-off using high-fidelity thermochemical models and the one-dimensional turbulence model, Proceedings of the Combustion Institute 35 (2015) 2829–2837.

[29] A. L. Brown, T. H. Fletcher, Modeling soot derived from pulverized coal, Energy and Fuels 12 (1998) 745–757.

[30] A. J. Josephson, D. O. Lignell, A. L. Brown, T. H. Fletcher, Revision to Modeling Soot Derived from Pulverized Coal, Energy and Fuels 30 (2016) 5198–5199.

[31] J. J. Murphy, C. R. Shaddix, Combustion kinetics of coal chars in oxygen-enriched environments, Combustion and Flame 144 (2006) 710–729.

[32] B. Goshayeshi, J. C. Sutherland, A comparative study of thermochemistry models for oxy-coal combustion simulation, Combustion and Flame 162 (2015) 4016–4024.

[33] L. Tognotti, J. P. Longwell, A. F. Sarofim, The products of the high temperature oxidation of a single char particle in an electrodynamic balance, Symposium (International) on Combustion 23 (1991) 1207–1213.

[34] A. D. Lewis, T. M. Holland, N. R. Marchant, E. G. Fletcher, D. J. Henley, E. G. Fuller, T. H. Fletcher, Steam gasification rates of three bituminous coal chars in an entrained-flow reactor at pressurized conditions, Energy and Fuels 29 (2015) 1479–1493.

[35] Babak Goshayeshi, Coal combustion simulation using one-dimensional turbulence model, Ph.D. thesis, The University of Utah, 2014.

[36] M. A. Hansen, J. C. Sutherland, Dual timestepping methods for detailed combustion chemistry, Combustion Theory and Modelling 21 (2017) 329–345.

[37] C. Bowman, R. Hanson, D.F. Davidson, W. J. V. Lissianski, G. Smith, D. Golden, M. Frenklach, M. Goldenberg, 1997.

[38] J. G. Wunning, J. A. and Wunning, Flameless oxidation to reduce thermal NO-formation, Progress in Energy and Combustion Science 23 (1997) 23, 81–94.

[39] C. Rottier, C. Lacour, G. Godard, B. Taupin, L. Porcheron, R. Hauguel, S. Carpentier, A. M. Boukhalfa, D. Honoré, On the effect of air temperature on MILD combustion flameless combustion regime of high temperature furnace, Proceedings of the European Combustion Meeting (2009).

[40] G. G. Szegö, B. B. Dally, G. J. Nathan, Operational characteristics of a parallel jet MILD combustion burner system, Combustion and Flame 156 (2009) 429–438.